EXPERIMENTAL STUDY OF REVERSE TAPERING AND RESONANCE DETUNING IN A SEEDED X-RAY FEL

L. Cao*, S. Liu, T. Long, E. Schneidmiller, J. Wu,
Deutsches Elektronen-Synchrotron DESY, Hamburg, Germany
G. Geloni, G. Perosa, European X-Ray Free-Electron Laser, Schenefeld, Germany

Abstract

Reverse tapering can suppress the FEL field while preserving electron microbunching for downstream radiators over an appropriate range of taper strength. In a monochromatically seeded FEL, one-dimensional small-signal theory suggests that the response to reverse tapering can be compared with the response to an accumulated resonance detuning. Here, we report on an experimental investigation of the relationship between undulator reverse tapering and resonance detuning in a seeded hard X-ray FEL, where the fixed seed frequency eliminates the influence of SASE photon-energy jitter. A modulator-radiator configuration was used in which U19 to U24 were scanned either by changing the resonance setting or by applying reverse tapering, while U25 was kept as the downstream radiator. The scans were performed with U25 active, to characterize the bunching-driven radiator signal, and with U25 off, to characterize residual upstream radiation. The U25-active spectra comparison shows a good agreement between reverse tapering and resonance detuning. The U25-off spectra show a stronger reduction of residual upstream radiation on the negative-detuning side than the U25-active radiator signal, indicating that the radiation field is suppressed more efficiently than the bunching-related signal, as expected for reverse-taper operation.

INTRODUCTION

High-purity circular polarization in X-ray FELs can be obtained by combining a planar main undulator with a short helical afterburner, provided that the linearly polarized background from the main undulator is sufficiently suppressed and the electron density modulation is preserved. Reverse tapering was proposed for this purpose and was shown to reduce the FEL field by orders of magnitude while maintaining substantial bunching over an appropriate taper range [1–3].

Both reverse tapering and resonance detuning modify the local resonance condition of the beam. However, their relationship is not obvious because reverse tapering produces an accumulated detuning, whereas a resonance-detuning scan applies a direct offset to the whole scanned section. Establishing how these two controls are related is important for understanding reverse-taper operation and for optimizing afterburner schemes. In SASE reverse-taper operation, although the amplified radiation frequency remains close to the resonance condition near the entrance of the tapered section, it is not fixed because of the intrinsic shot noise. In a monochromatically self-seeded FEL, by contrast, the reference frequency is fixed by the narrow-band seed. This allows the same downstream undulator section to be scanned in two controlled and comparable ways: by imposing a direct resonance offset relative to the seed frequency, or by applying a reverse taper.

In addition to the overall scale between taper strength and resonance detuning, the sign of the equivalent detuning is also expected to matter. One-dimensional small-signal theory suggests an asymmetric response with respect to the detuning sign. In the theory, the radiation field amplitude $\tilde{E}$ obeys a third-order linear differential equation. With the trial solution $\tilde{E} \propto \exp(\Lambda\hat{z})$, the corresponding dispersion relation can be written as [4]

$$\Lambda\left[(\Lambda + iC)^2 + \hat{\Lambda}_p^2\right] = i, \tag{1}$$

where C is the detuning parameter and $\hat{\Lambda}_p$ is the normalized coupling parameter. This dispersion relation is not invariant under C to $-C$, and therefore the eigenvalues and the linear propagation matrix of the seeded FEL amplifier are different for the two detuning signs. Since the density modulation, or bunching, is related to the field derivative $\tilde{E}'$, the bunching at the radiator entrance is not expected to satisfy $b(C) = b(-C)$.

Here, we compare reverse tapering and resonance detuning in the linear-gain regime of hard X-ray self-seeding (HXRSS) operation [5, 6] at the European XFEL [7]. The goal is to determine whether the reverse-taper response can be represented by an equivalent detuning offset and to compare the behavior of the bunching-driven radiator signal with the residual upstream radiation.

EXPERIMENTAL METHOD AND SCALING

As shown in Fig. 1, the measurement was performed in SASE2 of the European XFEL after optimizing HXRSS performance. Upstream undulator cells are used to generate SASE radiation, which is filtered by the forward Bragg diffraction crystal to produce the monochromatic seed wake. The weak chicane can be used to delay the electron bunch to overlap with the seed and wash out upstream microbunching.

A gain curve scan, in which the last active downstream cell was removed one by one, was used to choose a modulator-radiator configuration with the radiator placed before saturation. As shown in Table 1, the seeded signal changes weakly up to cell 21, grows rapidly from cell 22 to cell 25, and starts to level off by cell 26. Therefore, U19 to U24 were used as the scanned section and U25 setting was fixed to be used as

* l.cao@desy.de

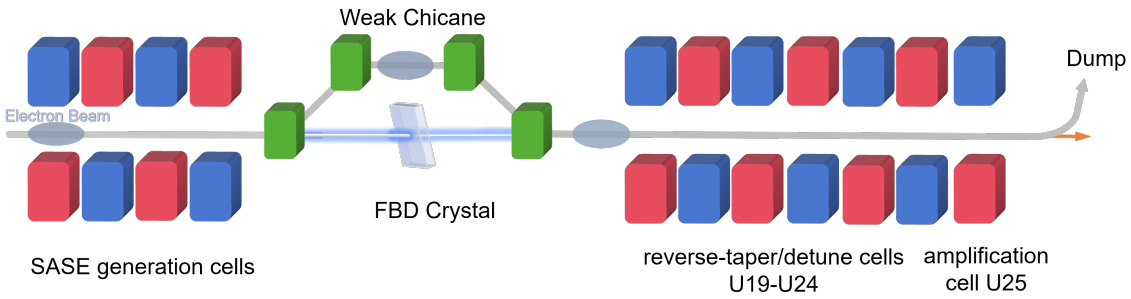

Figure 1: Schematic layout of the HXRSS resonance-detuning and reverse-taper measurements. U19 to U24 were scanned either by changing the resonance setting or by applying reverse tapering. U25 was used as the downstream radiator.

the final radiator. In the resonance-detuning scan, the undulator resonance photon-energy setting of the scan section was varied around the HXRSS seed energy of 7513 eV. In the reverse-taper scan, the linear taper setting of the same cells was varied while the resonance setting of the first scanned cell was kept fixed. Both scans were repeated with U25 active and with U25 off, and the spectra were recorded with the High-Resolution Hard X-ray spectrometer [8, 9].

Table 1: HXRSS gain scan. The seeded signal is calculated through the spectral integral averaged over 200 pulses

Last active cell	Seeded spectral integral (a.u.)
20	20
21	23
22	90
23	460
24	1100
25	1900
26	2200

The U25-active measurement is used to quantify the scaling between these two scan parameters as U25 converts the seeded microbunching into a measurable radiator signal in the linear gain regime. The U25-off measurement records radiation already generated from the scan section and is used to assess residual radiation.

The expected scale can be estimated from the undulator resonance condition. For a planar undulator, the resonant wavelength is

$$\lambda_r = \frac{\lambda_u}{2\gamma^2}\left(1 + \frac{K^2}{2}\right), \tag{2}$$

where λ_u is the undulator period, γ is the electron Lorentz factor, and K is the undulator parameter. Since $E_\gamma = hc/\lambda_r$, at fixed electron energy and undulator period, a small change of K gives

$$\frac{\Delta K}{K} = -\frac{1 + K^2/2}{K^2}\frac{\Delta E}{E_0}, \tag{3}$$

where E_0 is the photon energy at resonance.

In the experiment, the reverse-taper control value T denotes the linear cell-to-cell relative change of the undulator parameter, in units of 10^{-5}, with respect to the scan reference. The reverse-taper control value T can be converted to an equivalent detuning offset through a fitted coefficient α,

$$T = \alpha \Delta E_{\mathrm{exp}}. \tag{4}$$

Expressing $\Delta K/K$ in units of 10^{-5}, the resonance-based taper-to-detuning scale is

$$s_{\mathrm{th}} = 10^5 \left|\frac{\Delta K/K}{\Delta E}\right| = 10^5 \frac{1 + K^2/2}{K^2}\frac{1}{E_0}. \tag{5}$$

For $E_0 = 7513$ eV, $\lambda_u = 40$ mm, and an electron beam energy of 14 GeV, Eq. (2) gives $K \simeq 3.22$. Equation (5) then gives $s_{\mathrm{th}} \simeq 7.9\,\mathrm{eV}^{-1}$. If a section with an effective accumulated taper cell number N_{eff} follows the nominal resonance relation, then $N_{\mathrm{eff}} = s_{\mathrm{th}}/\alpha$.

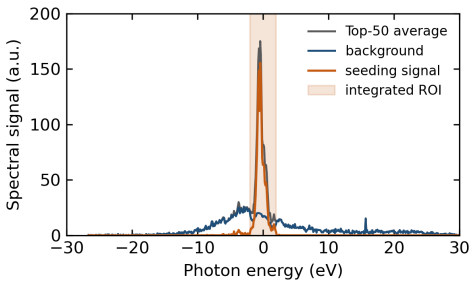

Figure 2: Example of background subtraction and spectral integration for the seeded signal. The gray curve shows the average spectrum of the top 50 selected pulses, the blue curve shows the estimated spectral background, and the orange curve shows the background-subtracted seeded signal. The shaded region indicates the photon-energy interval used for integration.

RESULTS

The analysis was based on the photon spectra rather than on the total pulse energy, in order to isolate the seeded spectral component from broadband SASE background and other radiation contributions. For each scan point, the spectra of 1000 pulses were ranked by their maximum spectral intensity and the 50 strongest pulses were selected. This selection procedure was applied identically to all scan points to reduce sensitivity to weak seeded shots caused by upstream SASE pulse-to-pulse jitter. The qualitative profile shape was stable against reasonable changes of the selected pulse number.

For each selected spectrum, a local baseline was estimated along the photon-energy axis with a rolling quantile filter

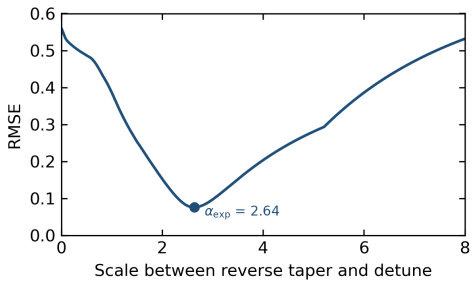

Figure 3: RMSE between the U25-active resonance-detuning and reverse-taper profiles as a function of the effective accumulated taper scale. The minimum gives $\alpha_{exp} \simeq 2.64\ \mathrm{eV}^{-1}$, corresponding to $N_{eff} \simeq 3$.

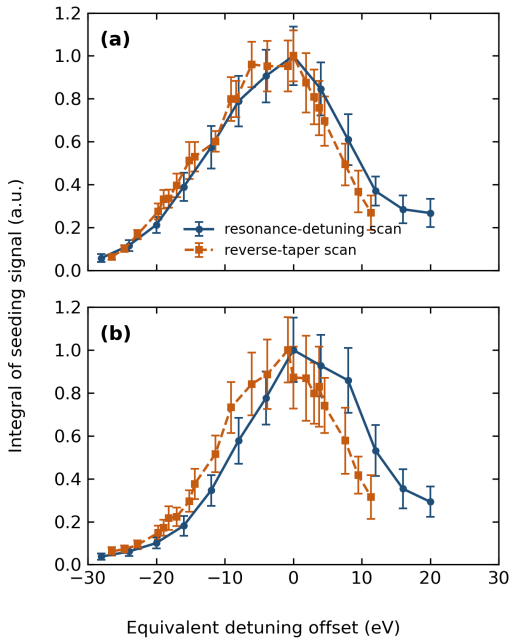

Figure 4: Comparison of the resonance-detuning scan and the reverse-taper scan for HXRSS after applying the best-overlap scale. (a) shows U25 active, where the final radiator converts the seeded modulation into a radiation signal. (b) shows U25 off, giving the residual upstream radiation from U19 to U24. The profiles are normalized to their maxima. The reverse-taper coordinate is converted to equivalent detuning offset using the fitted coefficient α_{exp}.

and subtracted point by point. The signal region was defined by a region of interest (ROI) centered on the seed photon energy with a half width of 2 eV. This width covers the seeded spikes observed in the spectra. Within the ROI, the baseline used for subtraction is the local quantile estimate evaluated under the seeded feature. The background-subtracted spectrum was then integrated over the ROI. Figure 2 illustrates the background-subtraction and integration method for the resonance-detuning setting at 7486 eV as an example.

For each scan mode and U25 setting, the spectral integral was normalized to its own maximum before comparing the resonance-detuning and reverse-taper dependences. The normalized profiles therefore test the profile shape and the mapping from reverse taper to equivalent detuning offset, rather than the absolute radiation suppression factor. The coefficient α was determined by minimizing the root-mean-square error (RMSE) between the interpolated U25-active resonance-detuning and reverse-taper profiles over their common equivalent-detuning-offset range.

The scale scan is shown in Fig. 3. The minimum corresponds to $\alpha_{exp} \simeq 2.64\ \mathrm{eV}^{-1}$. Comparing α_{exp} with $s_{th} \simeq 7.9\,\mathrm{eV}^{-1}$ gives $N_{eff} = s_{th}/\alpha_{exp} \simeq 3.0$. Thus, although the nominal scan covered U19 to U24, the fitted coefficient can be interpreted as an effective accumulated taper length of about three cells. This interpretation is consistent with the gain scan in Table 1. The gain scan does not directly measure the taper sensitivity of each cell, but it indicates where the seeded interaction becomes significant. It therefore suggests that the U25-active response is weighted toward the cells where the seeded gain is strongest, namely the downstream part of the scanned section, rather than uniformly over the full nominal length.

After applying the best-overlap coefficient α_{exp}, the U25-active resonance-detuning and reverse-taper profiles show good overlap, as shown in Fig. 4(a). For the normalized U25-active response under the present seeded conditions, this indicates that the reverse-taper scan can be approximately represented by an equivalent resonance-detuning coordinate. The response is asymmetric with respect to the detuning sign, which is consistent with the theoretical expectation. On the negative-detuning side, the U25-active signal decreases more rapidly than on the positive side.

The U25-off profiles in Fig. 4(b) exhibit a stronger decrease on the negative-detuning side than the U25-active profiles. Since the U25-off signal is sensitive to radiation generated upstream of U25, whereas the U25-active signal contains the additional radiator contribution driven by the microbunching delivered to U25, this difference suggests that the upstream radiation field is suppressed more strongly than the bunching-related radiator signal both for reverse-tapering and negative resonance-detuning. This observation is qualitatively consistent with the reverse-taper mechanism required for afterburner operation.

CONCLUSION AND DISCUSSION

A resonance-detuning scan and a reverse-taper scan were compared experimentally in the same undulator section of a monochromatically seeded hard X-ray FEL. In the experiment, these two scan parameters give the best profile overlap for $\alpha_{exp} \simeq 2.64\ \mathrm{eV}^{-1}$, corresponding to an effective accumulated taper length of about three cells when compared with the resonance-based scale $s_{th} \simeq 7.9\,\mathrm{eV}^{-1}$. The U25-off spectra show a stronger reduction of residual upstream radiation on the negative-detuning side. These observations support the equivalent-detuning-offset representation of the seeded reverse-taper response and provide an experimental benchmark for the reverse-taper operation. In the future, a direct comparison with SASE reverse-taper operation can also be conducted to study how the picture changes when the radiation frequency is no longer fixed by the seed.

REFERENCES

[1] E. A. Schneidmiller and M. V. Yurkov, "Obtaining high degree of circular polarization at x-ray free electron lasers via a reverse undulator taper", *Phys. Rev. Spec. Top. Accel. Beams*, vol. 16, p. 110702, 2013. doi:10.1103/PhysRevSTAB.16.110702

[2] A. A. Lutman *et al.*, "Polarization control in an X-ray free-electron laser", *Nature photonics*, vol. 10, no. 7, pp. 468–472, 2016. doi:10.1038/nphoton.2016.79

[3] E. Schneidmiller, M. Yurkov, *et al.*, "Reverse undulator tapering for polarization control and background-free harmonic production in XFELs: results from FLASH", in *Proc. International Free Electron Laser Conference (FEL'17)*, Santa Fe, NM, USA, pp. 20–25, Aug. 2017. doi:10.18429/JACoW-FEL2017-MOP032

[4] E. L. Saldin, E. Schneidmiller, and M. V. Yurkov, *The physics of free electron lasers*. Springer Science & Business Media, 2013.

[5] S. Liu *et al.*, "Cascaded hard X-ray self-seeded free-electron laser at megahertz repetition rate", *Nature Photonics*, vol. 17, no. 11, pp. 984–991, 2023. doi:10.1038/s41566-023-01305-x

[6] S. Liu *et al.*, "Updates on the Hard X-Ray Self-Seeding at the European XFEL", *Synchrotron Radiation News*, vol. 38, no. 2, pp. 11–16, 2025. doi:10.1080/08940886.2025.2472607

[7] W. Decking *et al.*, "A MHz-repetition-rate hard X-ray free-electron laser driven by a superconducting linear accelerator", *Nature photonics*, vol. 14, no. 6, pp. 391–397, 2020. doi:10.1038/s41566-020-0607-z

[8] N. Kujala *et al.*, "Hard x-ray single-shot spectrometer at the European X-ray Free-Electron Laser", *Rev. Sci. Instrum.*, vol. 91, no. 10, 2020. doi:10.1063/5.0019935

[9] N. Kujala *et al.*, "Commissioning of the SASE2 beamline single-shot spectrometer at the European X-ray free-electron laser", *J. Instrum.*, vol. 21, no. 03, P03047, 2026. doi:10.1088/1748-0221/21/03/P03047